Myocardial infarction quantification with Manganese-Enhanced MRI (MEMRI) in mice using a 3T clinical scanner

Article *in* NMR in Biomedicine · June 2010

DOI: 10.1002/nbm.1489 · Source: PubMed

6 authors, including:

Bénédicte MA Delattre
Hôpitaux Universitaires de Genève
69 PUBLICATIONS **775** CITATIONS
SEE PROFILE

Vincent Braunersreuther
University of Geneva
71 PUBLICATIONS **2,419** CITATIONS
SEE PROFILE

Jean-Noël Hyacinthe
Haute école de santé Genève
49 PUBLICATIONS **465** CITATIONS
SEE PROFILE

Lindsey Crowe
University of Geneva
48 PUBLICATIONS **1,014** CITATIONS
SEE PROFILE

Research Article

NMR IN BIOMEDICINE

Received: 2 July 2009, Revised: 13 November 2009, Accepted: 14 November 2009, Published online in Wiley InterScience: 19 February 2010

(www.interscience.wiley.com) DOI:10.1002/nbm.1489

Myocardial infarction quantification with Manganese-Enhanced MRI (MEMRI) in mice using a 3T clinical scanner

Bénédicte M. A. Delattre[a]*, Vincent Braunersreuther[b], Jean-Noël Hyacinthe[a], Lindsey A. Crowe[a], François Mach[b] and Jean-Paul Vallée[a]

Manganese (Mn^{2+}) was recognized early as an efficient intracellular MR contrast agent to assess cardiomyocyte viability. It had previously been used for the assessment of myocardial infarction in various animal models from pig to mouse. However, whether Manganese-Enhanced MRI (MEMRI) is also able to assess infarction in the acute phase of a coronary occlusion reperfusion model in mice has not yet been demonstrated. This model is of particular interest as it is closer to the situation encountered in the clinical setting. This study aimed to measure infarction volume taking TTC staining as a gold standard, as well as global and regional function before and after Mn^{2+} injection using a clinical 3T scanner. The first step of this study was to perform a dose-response curve in order to optimize the injection protocol. Infarction volume measured with MEMRI was strongly correlated to TTC staining. Ejection fraction (EF) and percent wall thickening measurements allowed evaluation of global and regional function. While EF must be measured before Mn^{2+} injection to avoid bias introduced by the reduction of contrast in cine images, percent wall thickening can be measured either before or after Mn^{2+} injection and depicts accurately infarct related contraction deficit. This study is the first step for further longitudinal studies of cardiac disease in mice on a clinical 3T scanner, a widely available platform. Copyright © 2010 John Wiley & Sons, Ltd.

Keywords: manganese; mouse; cardiac MRI; occlusion reperfusion; myocardial infarction; 3T

INTRODUCTION

In cardiac magnetic resonance imaging (MRI), extracellular contrast agents such as various gadolinium (Gd^{3+}) chelates, are now routinely used in clinical practice, as well as in research protocols to assess myocardial perfusion or interstitial space remodeling (1–3). Intracellular MR contrast agents can provide additional information on the cellular metabolism. Manganese ion (Mn^{2+}) was quickly recognized as an efficient intracellular MR contrast agent as it enters excitable cells via L-Type voltage dependant channels to accumulate in mitochondria and also induces a strong T1 shortening effect (4). As an analog of the Calcium ion (Ca^{2+}), Mn^{2+} can assess Ca^{2+} homeostasis *in-vivo* generating an important interest for researchers (5). In fact, Ca^{2+} cycling is of vital importance to cardiac cell function and plays an important role in ventricular dysfunction such as heart failure (6). Many conditions can influence the Mn^{2+} uptake by cardiomyocytes. The presence of dobutamine (which is known to increase Ca^{2+} influx into the heart) during Mn^{2+} infusion increases signal enhancement in T1-weighted images whereas the calcium channel blocker diltiazem reduces it (7). A reduced Mn^{2+} accumulation has also been observed in stunned cardiomyocytes (8) as well as in the zone adjacent to a myocardial infarct (5). Manganese-Enhanced MRI (MEMRI) has also been used to assess myocardial infarction in various animal models from pig to rat (9–12). Only a few studies, however, investigated the possible use of MEMRI for myocardial infarction assessment in mice (5,13). All of these studies used a model of permanent coronary occlusion. In this mouse model, infarct size determined by TTC at 7 days was linearly correlated to the infarct size measured from MEMRI (13) but a lower signal intensity, suggesting a decreased Mn^{2+} accumulation was also observed in the peri-infarct area where ischemic tissue may also be present (5). The type of coronary occlusion model, as well as the timing of examination after the induction of the myocardial injury, may also impact MEMRI experiments. By comparison to permanent coronary occlusion, the occlusion reperfusion model is closer to the clinical situation in which the occluded coronary artery is ultimately reperfused. The occlusion reperfusion model also induces a reduced myocardial remodeling and infarct size expansion in comparison to permanent occlusion (14) which can

* *Correspondence to: B. M. A. Delattre, Department of Radiology – CIBM, Geneva University Hospital, Rue Gabrielle-Perret-Gentil, 4, 1211 Geneva 14, Switzerland. E-mail: benedicte.delattre@hcuge.ch*

a *B. M. A. Delattre, J.-N. Hyacinthe, L. A. Crowe, J.-P. Vallée*
Faculty of Medicine, University of Geneva, Geneva, Switzerland

b *V. Braunersreuther, F. Mach*
Division of Cardiology, Department of Medicine, University Hospital, Foundation for Medical Researchers, Geneva, Switzerland

Contract/grant sponsor: Swiss National Science Foundation; contract/grant number: PPOOB3-116901.
Contract/grant sponsor: The Center for Biomedical Imaging (CIBM), Lausanne and Geneva, Switzerland.

Abbreviations used: *BW, body weight; CNR, contrast to noise ratio; EDV, end-diastolic volume; EF, ejection fraction; ESV, end-systolic volume; IP, intraperitoneal; IV, intravenous; MEMRI, manganese-enhanced MRI; MI, myocardial infarct; PSIR, phase-sensitive inversion recovery; ROI, region of interest; SI, signal intensity; TTC, triphenyltetrazolium chloride.*

affect Mn^{2+} uptake. Massive proliferation of fibroblasts and collagen deposition begins 7 days after the induction of myocardial infarct (15) whereas acute conditions are encountered 1 day after infarction, where inflammation and stunning prevails. Whether MEMRI is also able to assess myocardial infarct or a larger area including peri-infarct stunned myocardium in the acute phase in a mouse model of coronary occlusion reperfusion is largely unknown. Therefore, the purpose of this study was to investigate the use of MEMRI in the assessment of acute myocardial infarct in a clinically relevant coronary occlusion reperfusion model in mice.

The secondary aim of this study was the set up of a MEMRI protocol to assess subendocardial myocardial infarction on a 3T clinical MR scanner. The infarction model was chosen to be a 60 min coronary occlusion followed by 24 h of reperfusion. As Mn^{2+} toxicity is known to be a critical point (16), a dose response study was performed in order to maximize the enhancement provided for infarction quantification by injecting an optimal dose of Mn^{2+} without suffering from side effects [as arrhythmia, somnolence with general depressed activity, ataxia and respiratory stimulation (16)]. Cardiac function measurements were also performed systematically before and after Mn^{2+} injection in order to determine if the presence of Mn^{2+} alters the results. Finally this study aims to provide an efficient tool for further research in myocardial disease in mice as the MR system used in this experiment is a clinical scanner much more available than dedicated small animal MR systems.

METHODS

Animal preparation

15–20 week old C57BL/6J mice were anaesthetized with 4% isoflurane and intubated. Mechanical ventilation was performed (150 μl at 120 breaths/min) using a rodent respirator (model 683; Harvard Apparatus). Anaesthesia was maintained with 2% isoflurane delivered in 100% O_2 through the ventilator. A thoracotomy was performed and the pericardial sac was then removed. An 8–0 prolene suture was passed under the left anterior descending (LAD) coronary artery at the inferior edge of the left atrium and tied with a slipknot to produce occlusion. A small piece of polyethylene tubing was used to secure the ligature without damaging the artery. Ischemia was confirmed by the visualization of blanching myocardium, downstream of the ligation. After 60 min of ischemia, the LAD coronary artery occlusion was released and reperfusion occurred. Reperfusion was confirmed by visible restoration of color to the ischemic tissue. The chest was then closed and air was evacuated from the chest cavity. The ventilator was then removed and normal respiration restored. This group is named IR60 in the following ($n = 6$). Sham operated animals were subjected to the same protocol without LAD coronary occlusion ($n = 4$). Animals from the control group did not experience any surgery before MRI exam ($n = 4$). Twenty-four hours after surgical procedure, animals were submitted to MRI analysis and then sacrificed to perform histological staining as described in 'ex-vivo evaluation of infarct size' section.

Manganese injection protocol

$MnCl_2$ was diluted in NaCl 0.9% solution to obtain stock solution of 7.5 mM or 15 mM depending on the experiment. An intraperitoneal (IP) line was placed in the mouse before MRI exam in order to deliver the Mn^{2+} solution. To optimize the injection protocol we performed dose versus signal enhancement curves in control mice for several values of Mn^{2+} concentrations. Table 1 summarizes the concentrations and settings used for these injections. All settings were calculated in order to inject a maximum volume of 1 ml of stock solution. We measured signal enhancement in the septum as well as in the left ventricle free wall (around the anterolateral area, where infarction usually occurs with this model) to ensure that results were not dependent on the localization in the myocardium. Following the dose response results obtained, Mn^{2+} concentration delivered in the infarction quantification protocol was chosen to be 200 nmol/g body weight (BW) at a rate of 4 ml/h, typical infusion duration was 6 min for a 30 g BW mouse and the volume injected was 400 μl.

Table 1. Mn^{2+} injection parameters and heart rate (HR) measured at least 15 min after the end of Mn^{2+} injection for 'low' and 'high' concentrations experiments and general information about Mn^{2+} solution used in the measurement of dose *vs* signal enhancement curve. Symbols in brackets denote significant difference in HR compared with beginning of the experiment, before any Mn^{2+} injection (§$p < 0.01$, non stated values mean non-significant difference)

Low concentrations					High concentrations				
Stock solution 7.5 mmol/l					Stock solution 15 mmol/l				
experimental timing (min)	cumulative dose (nmol/g)	infusion time (min)	HR (bpm)	n	experimental timing (min)	cumulative dose (nmol/g)	infusion time (min)	HR (bpm)	n
0	0		333 ± 16	3	0	0		303 ± 27	4
5	35	4.2	311 ± 14	3	5	250	15	284 ± 6	2
40	70	4.2	306 ± 10	3	40	320	4.2	264 ± 38	2
75	100	3.6	298 ± 14	3	75	390	4.2	252 ± 30	4
110	150	6	289 ± 18 (§)	3	110	480	5.4	245 ± 39 (§)	4
145	200	6	290 ± 17 (§)	3					
infusion rate 2 ml/h									

NMR IN BIOMEDICINE

MR imaging

During the MRI exam mice were anesthetized with isoflurane 1–2%. Imaging was performed on a clinical 3T MR scanner (Magnetom TIM Trio, Siemens Medical Solutions, Erlangen Germany) with a dedicated 2-channel mouse receiver coil (Rapid biomedical GmbH, Rimpar Germany) 24 h after reperfusion. A turboflash cine sequence assessed myocardial function before and after Mn^{2+} injection: FOV 66 mm, in plane resolution 344 μm, slice thickness 1 mm, typically 4 consecutive slices to cover the whole left ventricle (no slice overlap), TR/TE 11/5 ms, flip angle 30°, GRAPPA with acceleration factor 2, 3 averages, typical acquisition time per slice 3 min. A T1-weighted turboflash sequence using Phase Sensitive Inversion Recovery reconstruction (PSIR) (17) assessed myocardial viability: FOV 80 mm, in plane resolution 156 μm, slice thickness 1 mm, typically 8 slices (50% slice overlap), TR/TE 438/7.54 ms, flip angle 45°, TI 380 ms, GRAPPA with acceleration factor 2, 2 averages, typical acquisition time per slice 2 min 30. Fifty percent slice overlap was chosen to diminish effects of partial volumes (18). For this sequence a constant TI was chosen to keep the same contrast properties in all images. Both sequences were respiratory and ECG gated.

Ex-vivo evaluation of infarct size

After MR imaging, the mice were re-anaesthetized with 10 ml/kg of ketamine-xylazine (12 mg/ml and 1.6 mg/ml, respectively) and the animals were sacrificed by a rapid excision of the heart. The heart was then rinsed in NaCl 0.9%, frozen and manually sectioned into 1–2 mm transverse sections from apex to base (5–6 slices/heart). These slices were incubated at 37°C with 1% triphenyltetrazolium chloride (TTC) in phosphate buffer (pH 7.4) for 15 min, fixed in 10% formaldehyde solution and each side of the slices was photographed with a digital camera (Nikon Coolpix). The different zones (left ventricular wall myocardium and infarction) were determined using a computerized planimetric technique (MetaMorph v6.0, Universal Imaging Corporation). Animals from the control and sham groups were also submitted to histological staining after the MRI exam.

Image analysis

Ejection fraction (EF) calculation and infarction quantification were performed with Osirix software (Open source http://www.osirix-viewer.com/). For EF calculations, segmentation of the endocardial contour allowed evaluation of the end-diastolic volume (EDV) and end-systolic volume (ESV), with EF defined as (EDV-ESV)/EDV. Wall thickening evaluation for regional function assessment was done using in-house software allowing calculation of percentage wall thickening in sectors covering the whole left ventricle. Sectors were defined by the American Heart Association (AHA) standardized guidelines for myocardial segmentation (19). Figure 1 shows this segmentation. For the Mn^{2+} dose study and infarction quantification, segmentation was done by manually drawing a region of interest (ROI) in septum area, myocardial infarction (MI) or free wall. The mean ROI size was 1.22 ± 0.51 mm^2. The free wall ROI was chosen to be in the same myocardial area for the control and sham-operated groups as for the IR60 group. Infarction quantification was performed with a threshold technique and compared to the quantification performed with TTC staining, which is considered as a gold standard (20). For the IR60 group, the threshold was defined as the mean signal intensity (SI) measured in the myocardium area presenting a significant contractile dysfunction observed on cine images and a hypointense area on one representative slice (generally the middle slice of the heart). The error in estimation of the infarct volume was evaluated by defining the threshold obtained by repeated drawing of ROI in the same area. This deviation was 5 a.u. and was the same for all mice in this group. Infarction volume was then evaluated taking initial threshold ± 5 a.u. For the control and sham groups, the infarction volume was derived from the threshold of the IR60 group. In fact, we observed that infarction area had a SI reduction of 60 a.u. compared to septum area (mean taken for all IR60 mice, $n = 6$), so the threshold was defined as SIm-60 where SIm was the mean SI between 2 ROI (one in septum and one in free wall). Error bars were determined by evaluating infarction volume taking the deviation of 5 a.u. on the threshold as described for the IR60 group.

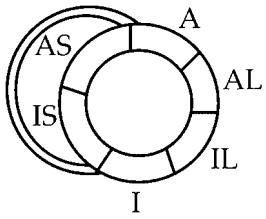

Figure 1. Myocardial segmentation as defined by the American Heart Association (17). Middle slice of the left ventricle is divided into six sectors: A = anterior, AL = anterolateral, IL = inferolateral, I = inferior, IS = inferoseptal, AS = anteroseptal.

Statistics

All values are quoted as mean ± standard deviation (SD). Statistics were performed with SPSS Statistics 17.0 software. To compare results of the three groups (control, sham operated and IR60) analysis of variance (ANOVA) was performed, followed by a Bonferroni post-hoc test. To compare results obtained before and after Mn^{2+} injection, a student's *t*-test was performed. The significance was set to $p < 0.05$.

RESULTS

Manganese dose determination

The first step of our study was to determine the lowest Mn^{2+} dose to deliver in order to have the best enhancement of the myocardium with our PSIR sequence while remaining under the toxic level. This was important considering the toxicity of Mn^{2+} at high concentrations and delivery rate (16) and the variability of the different doses reported in literature for cardiac MEMRI. We observed a maximal enhancement of the myocardium 45 min after Mn^{2+} injection. The results shown in Figure 2 indicate that signal enhancement increases linearly with Mn^{2+} dose up to 200 nmol/g before reaching a plateau. Linear regression results are $y = 0.78x - 26.37$ with $R^2 = 0.99$ and $p < 0.001$ for signal enhancement measured in septum area and $y = 0.81x - 21.77$ with $R^2 = 0.99$ and $p < 0.001$ for measurement in free wall. Slopes and intercepts are not significantly different between these two regions of interest ($p > 0.05$). No arrhythmia or significant change in heart rate were encountered at high Mn^{2+} concentrations when comparing with the heart rate just before Mn^{2+} injection ($p > 0.2$). However, for the

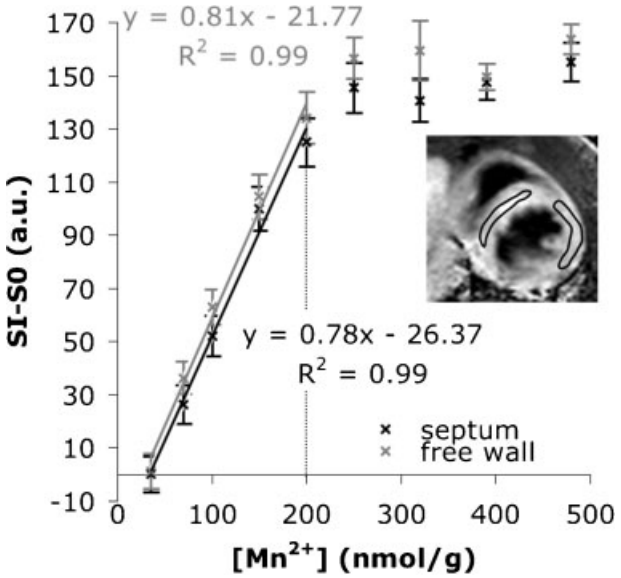

Figure 2. Signal enhancement measured in septum and free wall area (see insert) for control mice (signal intensity, SI, minus signal baseline measured before Mn^{2+} injection, S0) 45 min after Mn^{2+} injection versus Mn^{2+} dose.

'low' concentration as well as for the 'high' concentration experiments, the successive injections of Mn^{2+} led to a decrease of heart rate that became significant for the last doses when compared with the heart rate measured at the beginning of the experiment ($p < 0.03$ and $p < 0.05$ for 'low' and 'high' dose protocol respectively). We have to note that even for the highest dose (480 nmol/g) we were well below the acute toxicity limit that is 962 nmol/g for IP route (16). For the following experiments, i.e. infarction quantification, we choose an $MnCl_2$ IP injection of 200 nmol/g BW at a rate of 4 ml/h from a stock solution of 15 mmol/l (the stock solution of higher concentration was chosen in order to minimize the injected volume as well as the injection duration which was thus 400 μl and 6 min respectively for a 30 g mouse).

Infarct quantification

During each experiment, PSIR images of the whole myocardium were acquired. A typical example is shown in Figure 3 (upper row). Infarction area is represented as hypointense signal corresponding to a reduced uptake of Mn^{2+} compared to viable myocardium where Mn^{2+} accumulates. Contrast to noise ratios (CNR) between signal measured in MI area (or free wall) and septum area for the control, sham operated and IR60 groups were measured. Noise was chosen to be the mean of the SD in both those areas. For the IR60 group CNR was 4.00 ± 1.59 which is significantly higher ($p < 0.01$) than sham operated, 0.66 ± 1.04 and control groups, -0.13 ± 0.60. Also, no significant difference was found between the control and sham groups ($p = 1.000$), and both values are not significantly different from zero ($p = 0.7$ and $p = 0.3$ for control and sham respectively).

Figure 3 shows an example of the comparison between MEMRI and TTC staining. An ROI was drawn in the infarction area on MEMRI images as described in the Methods section, and the mean SI of this area defined the threshold used for infarction quantification. Figure 4 illustrates an example of this segmentation method. Infarction quantification performed with MEMRI is strongly correlated with the measurements derived from TTC staining, as shown by Figure 5. The error bars aim to indicate the maximal deviation that could be made by applying the segmentation method. The maximal deviation obtained was 9%. The result of linear regression was $y = 0.94x$ with $R^2 = 0.91$ and $p < 0.001$. The Bland-Altman plot also shows a good agreement between the two methods without significant bias. The mean of the differences between MEMRI and TTC is 1.7%. In both the control and sham operated groups, the signal intensity was homogenously enhanced over all the heart without any large

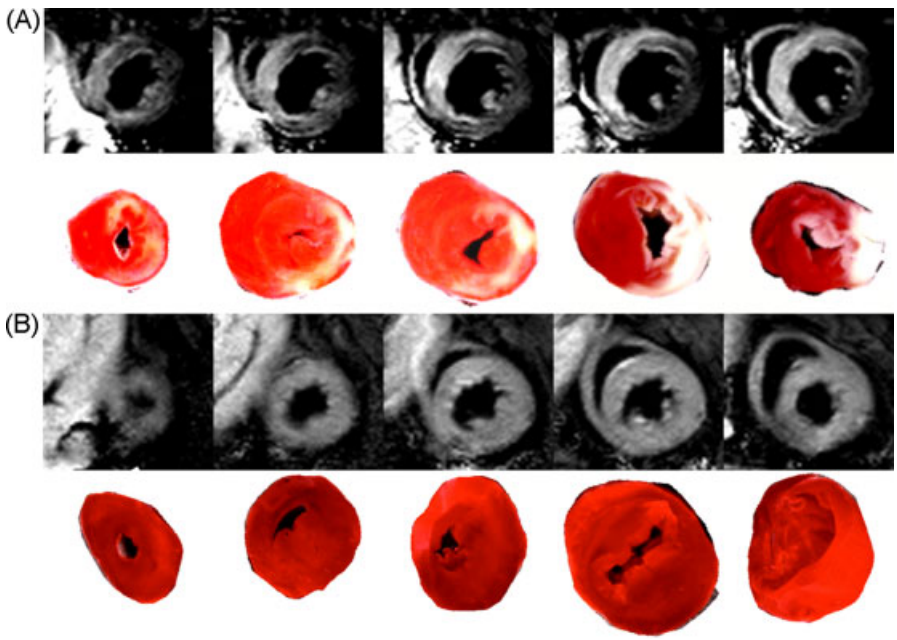

Figure 3. Selection of T1-weighted PSIR short axis images (upper row) and corresponding TTC staining (bottom row) for an IR60 mouse (A) and a sham operated mouse (B). White colour present in TTC slices for (A) indicating tissue necrosis correlates with hypointense signal in PSIR images whereas neither white nor hypointense signal is present in (B).

NMR IN BIOMEDICINE

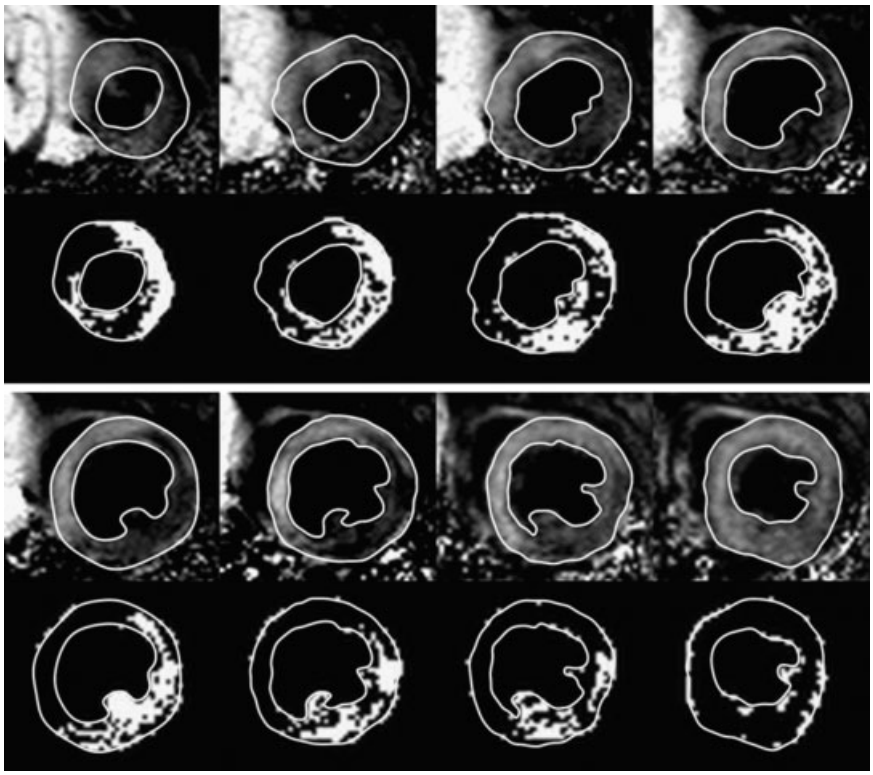

Figure 4. Segmentation method for infarction volume quantification. Upper row; example of slices covering whole heart of an IR60 mouse with manually drawn endocardial and epicardial contours. Bottom row; corresponding results of the threshold segmentation technique.

area of hypointense signal on the PSIR, as shown in Figure 3 and confirmed by the fact that CNR is not significantly different from zero for the control and sham groups respectively. This was in agreement with the TTC staining that did not reveal myocardial infarct in both these groups.

Function assessment

Cine slices covering the whole left ventricle were acquired in order to measure global and regional function before and after Mn^{2+} injection. Examples of cine images for the left ventricle middle slice of a control mouse and an IR60 mouse are given in Figure 6. We observed a clear contraction decrease for the IR60 mouse compared to the control mouse. Global function was determined by measurement of the ejection fraction (EF). Table 2 shows results of EDV, ESV, EF and heart rate for IR60, sham operated and control groups for measurements done before and after Mn^{2+} injection. We obtained a significant decrease of EF for the IR60 group compared to the sham (29%, $p < 0.01$) and control (20%, $p < 0.05$) groups before Mn^{2+} injection. However, these differences were no longer significant after Mn^{2+} injection. We could also note a significant decrease in EDV and ESV, leading to an increase in EF for the control group as well as a decrease in ESV for the IR60 group after Mn^{2+} injection. Heart rate was not significantly different neither between the three groups ($p > 0.4$) nor after Mn^{2+} injection ($p > 0.2$).

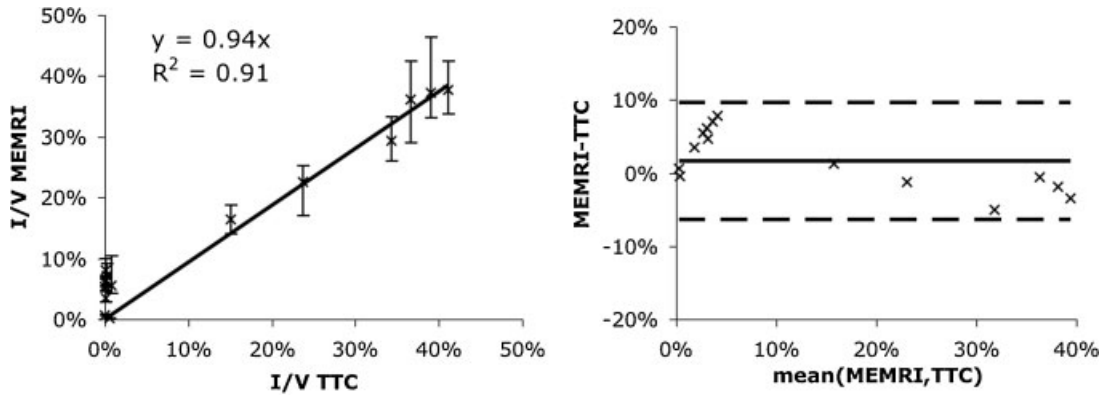

Figure 5. Left; infarction volume quantification with MEMRI versus TTC staining for IR60 ($n = 6$), sham ($n = 4$) and control ($n = 4$) groups as a percentage of left ventricular wall volume. Error bars symbolize the volume variation obtained with the threshold segmentation technique. Right; Bland–Altman plot for comparison of infarction quantification method between MEMRI and TTC staining. Solid line is mean(MEMRI-TTC) = 1.7%, dashed lines are 1.96*SD(MEMRI-TTC) = 8.0% corresponding to 95% Confidence Interval.

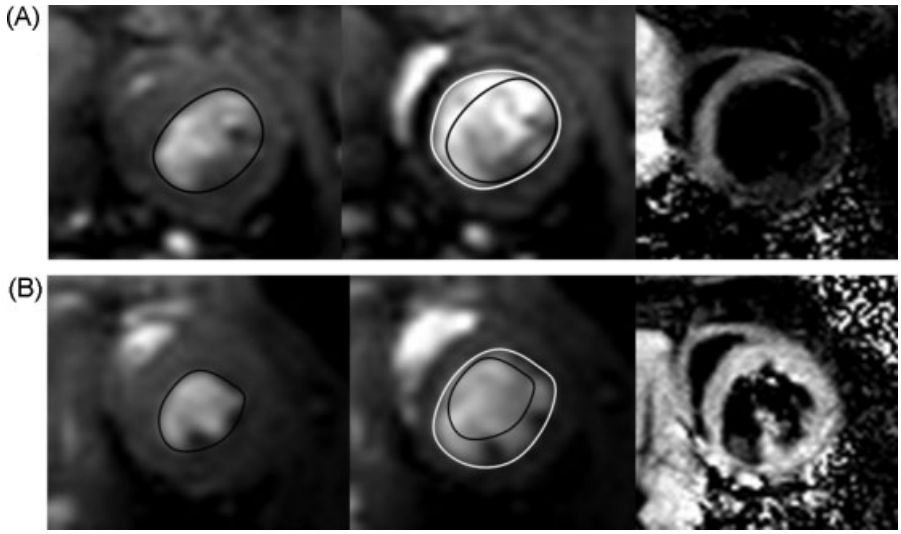

Figure 6. Example of cine images of systolic (left) and diastolic (middle) phases in middle slice of heart, as well as T1-weighted PSIR image (right) for an IR60 mouse (A) and a control mouse (B). In (A) the lateral part of the myocardium is not moving between systolic and diastolic phases which is not the case in (B).

Left ventricular regional function was assessed by comparing wall thickness between diastole and systole for 6 sectors covering the whole left ventricle, leading to percentage wall thickening evaluation. Figure 7 shows the results obtained before and after Mn^{2+} injection for control, sham operated and IR60 mice. Table 3 shows the mean wall thickening in the six different myocardial sectors for the three groups. Wall thickening was significantly reduced in every free wall area (including anterior, anterolateral, inferolateral and inferior sectors) for infarcted mice compared with the control and sham groups ($p < 0.001$ before Mn^{2+} injection and $p < 0.01$ after), while no significant difference was obtained in the septum sectors. As an example, before Mn^{2+} injection, wall thickening is 0.77 ± 0.12 in the anterolateral sector for the control group and is reduced to 0.11 ± 0.07 for the IR60 group, which constitutes a decrease of 86%. Also, no significant difference was measured, neither between control and sham groups ($p > 0.4$), nor between measurements done before and after Mn^{2+} injection ($p > 0.5$). Figure 8 shows the correlation between wall thickening and signal intensity for each sector of the left ventricle. To avoid any bias between mice, signal intensity was normalized to signal intensity of the anteroseptal sector. For the IR60 group we obtained a strong correlation between regional function and signal intensity, i.e. presence of Mn^{2+}, in different sectors ($y = 22.3x - 21.7$, $R^2 = 0.824$, $p = 0.01$). However, no correlation was found for the control ($R^2 = 0.003$, $p = 0.9$) and sham groups ($R^2 = 0.290$, $p = 0.3$).

DISCUSSION

Summary of results

As the main result of the study, a strong relationship, close to unity, was observed for the infarction volume measurement by MEMRI and TTC staining in the mouse model of acute myocardial infarct induced by an occlusion reperfusion. Global function could be assessed, as well as regional contraction deficit relative to infarction induction. As an additional result, we validated the use of a clinical 3T MR system for the study of myocardial infarct in mice by a careful optimization of the protocols including the dose and timing of the delivered Mn^{2+}, the cine and T1 weighted MR sequences.

Table 2. End diastolic volume (EDV), end systolic volume (ESV), ejection fraction (EF) and heart rate (HR) for IR60, sham and control groups, measured before and after Mn^{2+} injection. Values are mean ± SD. For the IR60 group, *P* indicates significant difference with the sham and control groups respectively obtained with post-hoc Bonferroni test (*$p < 0.05$; §$p < 0.01$; †$p < 0.001$). Symbols in brackets indicate result of *t*-test for comparison of measurement done before and after Mn^{2+} in each group

					P	
		IR60	sham	control	IR60 vs sham	IR60 vs control
EDV (μl)	before Mn	57.6 ± 9.5	30.7 ± 13.9	40.8 ± 6.1	§	NS
	after Mn	47.5 ± 10.8 (NS)	32.6 ± 3.2 (NS)	30.3 ± 4.1 (*)	NS	*
ESV (μl)	before Mn	30.9 ± 5.3	10.2 ± 5.4	16.6 ± 2.0	†	†
	after Mn	20.7 ± 5.1 (§)	8.4 ± 3.8 (NS)	8.7 ± 1.6 (†)	§	§
EF	before Mn	0.47 ± 0.06	0.66 ± 0.09	0.59 ± 0.03	§	*
	after Mn	0.57 ± 0.07 (NS)	0.75 ± 0.09 (NS)	0.71 ± 0.05 (§)	NS	NS
HR (bpm)	before Mn	328 ± 25	291 ± 53	348 ± 29	NS	NS
	after Mn	316 ± 42 (NS)	283 ± 37 (NS)	317 ± 33 (NS)	NS	NS

NMR IN BIOMEDICINE

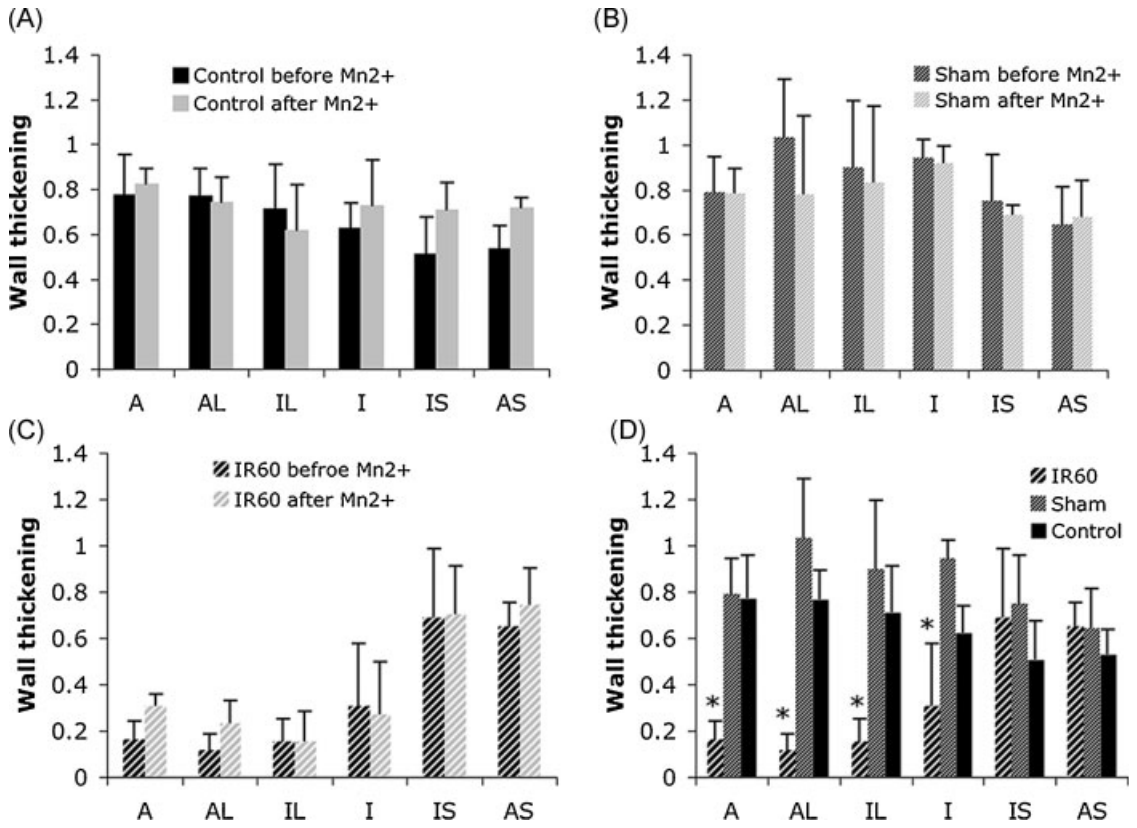

Figure 7. Wall thickening between diastolic and systolic phase for sectors defined in Figure 1 before and after Mn^{2+} injection, for control group ($n = 4$) (A), sham operated group ($n = 4$) (B), IR60 group ($n = 6$) (C), and comparison of wall thickening before Mn^{2+} injection for the 3 groups (D). Values are Mean ± SD (A = anterior, AL = anterolateral, IL = inferolateral, I = inferior, IS = inferoseptal, AS = anteroseptal). * indicates significant difference between groups (at least $p < 0.05$).

Table 3. Wall thickening between diastolic and systolic phase in the 6 left ventricle sectors (defined in Fig. 1) for IR60, sham and control groups, before and after Mn^{2+} injection. Values are mean ± SD. For the IR60 group, *P* indicates significant difference with the sham and control groups respectively obtained with post-hoc Bonferroni test (*$p < 0.05$; §$p < 0.01$; †$p < 0.001$)

				P	
Before Mn^{2+}	IR60	sham	control	IR60 vs sham	IR60 vs control
anterior	0.16 ± 0.08	0.79 ± 0.16	0.77 ± 0.18	†	†
anterolateral	0.11 ± 0.07	1.03 ± 0.26	0.77 ± 0.12	†	†
inferolateral	0.15 ± 0.10	0.90 ± 0.29	0.71 ± 0.20	†	§
inferior	0.31 ± 0.27	0.94 ± 0.08	0.63 ± 0.11	§	NS
inferoseptal	0.69 ± 0.30	0.75 ± 0.21	0.51 ± 0.17	NS	NS
anteroseptal	0.65 ± 0.10	0.64 ± 0.17	0.53 ± 0.11	NS	NS
				P	
After Mn^{2+}	IR60	sham	control	IR60 vs sham	IR60 vs control
anterior	0.31 ± 0.05	0.78 ± 0.11	0.82 ± 0.08	†	†
anterolateral	0.23 ± 0.10	0.78 ± 0.35	0.74 ± 0.11	§	§
inferolateral	0.15 ± 0.13	0.83 ± 0.34	0.62 ± 0.20	§	*
inferior	0.27 ± 0.23	0.92 ± 0.07	0.73 ± 0.20	†	§
inferoseptal	0.71 ± 0.21	0.69 ± 0.04	0.70 ± 0.13	NS	NS
anteroseptal	0.74 ± 0.16	0.68 ± 0.16	0.71 ± 0.05	NS	NS

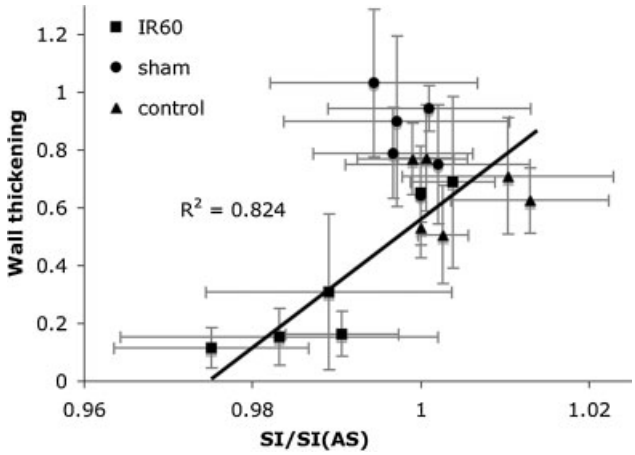

Figure 8. Wall thickening versus signal intensity for the 6 sectors covering the left ventricle (A = Anterior, AL = Anterolateral, IL = Inferolateral, I = Inferior, IS = Inferoseptal, AS = Anteroseptal). For each mouse, signal intensity of each sector was normalized to signal intensity of AS sector. Values are mean ± SD for IR60 ($n = 6$), sham ($n = 4$) and control group ($n = 4$). Linear fit and R^2 coefficient relates to the correlation obtained for IR60 group values.

Manganese dose determination

The Mn^{2+} dose-response study was necessary for two reasons. First, all previous studies on cardiac MEMRI in mice were done on a dedicated small animal system, either with a 9.4T (13) or a 7T magnet (5,7) which are known to give a better sensitivity and have higher gradient performances than clinical systems. We choose to work on a 3T magnet to take advantage of the implementation of clinical sequences and features like PSIR and GRAPPA. We reached a spatial and temporal resolution comparable to those used in other studies with the performance of this system. Secondly, we used a T1-weighted PSIR sequence to assess signal enhancement that is different from sequences used in those previous studies (FLASH or T1-mapping sequence). The inversion recovery (IR) sequence is the best choice for the assessment of myocardial injury in patients because of its high T1 sensitivity (21). However, image quality can be altered by an inappropriate choice of inversion time (TI). Phase sensitive reconstruction from the PSIR sequence prevents this problem and gives more consistent image quality than an IR sequence (17). A better consistency in data is expected with a T1-mapping sequence, however this kind of measurement is for the moment very long [around 45 min (5)].

During our experiments, we observed a maximal enhancement of viable myocardium 45 min after Mn^{2+} injection, therefore images for infarction quantification were taken after such a delay. This delay is in agreement with other previous studies (7,13) where injection was made intravenously (IV). This delay is mainly explained by the time necessary for Mn^{2+} ions to be accumulated in mitochondria after entering the cardiomyocytes via L-type calcium channels, as IP injection is comparable to IV in mice (22).

During the dose response experiments, heart rate measured at least 15 min after the end of each Mn^{2+} injection did not decrease significantly compared to before each injection. However, the heart rate decreased progressively during the experiment to finally become significantly different from the one measured at the beginning of the experiment, before the first injection. Knowing that Mn^{2+} plasma half-life is approximately 3 min (23), it suggests that the observed depression was more probably due to the cumulative effect of the anesthesia than to a direct effect of Mn^{2+} injection. This can be explained by the fact that anesthesia was driven in order to keep a stable respiratory rate and not necessarily a constant heart rate. Moreover, the decreased heart rate observed at the end of the 'low' concentrations protocol corresponding to 200 nmol/g of Mn^{2+} was not reproduced after the first injection of 250 nmol/g Mn^{2+} in the "high" concentrations protocol. The results in Table 2 confirm this hypothesis as no significant change in heart rate was measured after Mn^{2+} injection in each group (the dose used for infarction quantification was 200 nmol/g).

In Figure 2, a plateau of signal enhancement is reached for Mn^{2+} concentrations higher than 200 nmol/g. This plateau indicates either a saturation-related problem that does not allow visualization of a further increase in Mn^{2+} concentration in the myocardium after this level because of the limited dynamic of the SI or is a result of a true physiological effect. Indeed, significant shortening of T1 in tissue due to Mn^{2+} leads to a saturation of SI, dependent on the inversion time chosen in the sequence. The physiological effect could be due to either a limited Mn^{2+} accumulation in the cardiomyocytes or a limited relaxation rate change secondary to protein binding with Mn^{2+} ions. According to Kang *et al.* (24), binding of Mn^{2+} ions to macromolecules leads to a more efficient dipolar interaction with surrounding protons significantly decreasing proton T1. Our experiments could not answer this question as further investigations were beyond the scope of this study. However, a recent study of Waghorn *et al.* (5), who mapped the T1 decrease in myocardium, shows the same plateau in their measurements occurring above 197 nmol/g (which is comparable with our results). They came to the conclusion that above this concentration, an increase in Mn^{2+} concentration in the myocardium did not lead to a decrease in T1 even if the absolute concentration of Mn^{2+} in dry myocardium increased. This would tend to validate the hypothesis of a limited change in relaxation rates.

Infarction quantification

Gadolinium chelates are largely used for assessment of myocardial infarction in mouse models (1,25,26). However, even if this method has largely proven its efficiency, it has some disadvantages over Mn^{2+} late enhancement. First, the time window during which assessment is possible is relatively short with Gd^{3+} [around 1 h (25)] compared with Mn^{2+} where ions can stay in mitochondria for several hours (5). Also, performing infarct quantification too early with Gd^{3+} can lead to an overestimation of the infarct zone that restrains again this time window between 20 and 60 min after injection (25–27). From this point of view, Mn^{2+} allows more flexibility. Thirdly Mn^{2+} makes the viable part of myocardium appear bright which allows an easier segmentation of the myocardium and the infarct pattern than with Gd^{3+}, where parameters of the sequence are often chosen to null myocardium signal prior to contrast agent addition.

Comparing with other previous studies conducted at high field, gradient performances of our system allowed a similar spatial resolution [156 μm *vs* 117 μm at 11.7T (25) or 100 μm at 9.4T (28)] leading to a precise infarction quantification. Indeed, we obtained an excellent correlation with TTC measurement

NMR IN BIOMEDICINE

($y = 0.94x$, $R^2 = 0.91$), with no bias between methods confirmed by Bland–Altman plot. These results are very similar to those obtained with Gd^{3+} enhancement for the same infarction model (26). This was reinforced by CNR results that showed a strong contrast between viable and infarct area in the IR60 group but, as expected, not in the control and sham operated groups. The high variability obtained for CNR measurements can be explained by the method of noise calculation. The noise was estimated from the standard deviation of the SI in the left ventricle wall. It is therefore a physiological noise much higher than image noise that could be measured from an empty area of the images. However, CNR was always sufficiently high to allow infarction segmentation in the IR60 group.

These results did not bring to light any significant difference of Mn^{2+} uptake between control and sham group, indicating that the open chest surgical procedure do not affect Ca^{2+} homeostasis sufficiently to be detected by our method. However, in both control and sham groups, infarction quantification led to a non-zero value whereas TTC results did not indicate any necrosis. This was often caused by darker pixels present at edges of the myocardium that were counted as part of an infarct. Although, the erroneous pixels could be easily detected by visual inspection, we chose not to discard them but rather to use a linear model with no intercept in order to decrease the contribution of these isolated pixels. As a work in progress, a possible refinement of the method would be to apply morphological operations (erosions and dilatations) on the segmented images to eliminate contributions of isolated pixels at edges.

An important result was that MEMRI did not overestimate the infarct size. In fact, no previous study has described Mn^{2+} enhancement in acute phase of reperfused infarction, so it was not known whether other mechanism such as stunning could affect Mn^{2+} uptake. Very little literature is found on the assessment of stunning in mice (29,30) and no data is provided for our mouse model and time point (24 h after injury). However, Krombach *et al.* (8) have previously shown that Mn^{2+} can assess stunning in rats 30 min after repeated ischemia-reperfusion protocol. The explanation of such mechanism remains controversial as Mn^{2+} was accumulating via Na^+/Ca^{2+} exchanger-mediated transport during hypoxia in an in vitro study of isolated perfused myocardium (31). Should Mn^{2+} uptake be reduced in stunned cardiomyocytes, it could induce an overestimation of the infarction volume compared to TTC. Such an effect was clearly not present in our model. Finally, it was important to provide a running protocol to assess myocardial infarction in the acute phase as it is the start point of all further longitudinal studies.

Function assessment

As shown in Table 2, we obtained a significant decrease of EF for the IR60 group compared with the control and sham operated groups (20% $p < 0.05$ and 29% $p < 0.01$ respectively). However, when comparing EDV and ESV with another study for the same model (26) we have higher results in volume estimation leading to decreased EF for the control group [59% *vs* 70% (26)]. This could be due to the lower spatial resolution reached in our cine measurements [344 μm *vs* 100 μm (26)], but also to a deeper anesthesia of the animal. Indeed, it has been recently shown that, in control mice, isoflurane anesthesia can reduce EF to 60% relative to 79% obtained with a deep sedation only (32).

Also, compared to baseline, before Mn^{2+} injection, we obtained a global increase in EF measurements after Mn^{2+} injection that is significant for the control group and correlated with a decrease in EDV and ESV. This is explained by the loss of contrast between blood and myocardium in presence of Mn^{2+}. In fact, the determination of endocardial contours tends to be underestimated. From the definition of EF, if EDV and ESV are underestimated EF is therefore overestimated. As Mn^{2+} intake is globally more significant in control mice myocardium than in other groups it can explain the difference between measurements done before and after Mn^{2+} injection in this group. As a consequence, estimation of EF should preferentially be done before Mn^{2+} injection. However, we must point out that observations from cine images still show the presence, or not, of a decreased contraction after Mn^{2+} injection. Some flow artifacts are still present in cine images due to longer TE, especially at phases when a significant change in flow occurs, however those artifacts are far from the systolic and diastolic phases so they do not alter function quantification. Reduction of TE is limited by gradient performance, so a possible way to assess this problem would be to use a sequence that allows compensation of gradient moments such as spiral acquisitions (33).

Regional function showed a significant decrease in wall thickening from the anterior to the inferior part of the myocardium for the IR60 group compared to the control and sham groups. From Table 3 no significant difference was observed in wall thickening measurement between control and sham group. Moreover, globally no significant difference is obtained in measurements done before and after Mn^{2+}. This is explained by the fact that the underestimation of the endocardial contour affects this measurement less than for EDV and ESV, where this error is multiplied by the number of slices. To check this hypothesis, we measured the area of myocardium obtained by manually tracing endocardial and epicardial contours before and after Mn^{2+} injection. The area was not significantly different before and after injection for the systolic and diastolic phases in the IR60, sham and control groups (results not shown). This measurement can therefore be done after Mn^{2+} injection, which allows considerable acceleration of the imaging protocol by doing the injection 45 min before the MRI exam. Also, Figure 8 showed a strong correlation between wall thickening and normalized SI for each sector of the left ventricle showing that Mn^{2+} is mostly present in functional parts of the myocardium supporting the hypothesis that Mn^{2+} effectively depicts extracellular Ca^{2+} uptake through L-type channels. No correlation was found, either for sham, or for control groups due to the lack of dispersion of wall thickening and normalized signal intensity values. However, even if these results depicted the contraction deficit relative to infarction, an important improvement in function evaluation would be to perform assessment of intramyocardial strains, either by displacement-encoded imaging with stimulated echos (DENSE) (34) or with myocardial tagging, as was previously reported in rat myocardium (35) and also in mice (36,37). Moreover, it has been shown that myocardial tagging can also provide accurate EF measurement (38), so both regional and global function can be acquired in one single acquisition.

Further applications

This study shows the feasibility of acute infarction assessment and quantification at 3T. This opens various possibilities for

applications such as longitudinal studies of infarction evolution with different ischemic models, risk zone assessment as previously done in other animal models (18,39), and investigation of drug effect on infarction size. Indeed, in rats, injecting Mn^{2+} at the beginning of occlusion instead of after reperfusion led to an accumulation of ions in the well perfused myocardium, showing the area at risk as a hypointense signal in MEMRI (18). The ratio of infarct area over the risk zone could be accurately measured in mice with this method, thus decreasing the variability related to variation of the occlusion site and or coronary anatomy.

CONCLUSIONS

Infarction assessment in a mouse model of reperfused myocardial infarction in the acute phase of the injury with MEMRI has not previously been reported. This study has shown assessment and quantification of even non-transmural infarcts with an excellent correlation to standard TTC staining results. Ejection fraction and percentage wall thickening measurements allowed evaluation of global and regional function. While EF must be measured before Mn^{2+} injection to avoid bias introduced by the reduction of contrast in cine images, percent wall thickening can be measured either before or after Mn^{2+} injection and accurately depicts infarct-related contraction deficit. Finally, this MEMRI protocol allows longitudinal study of cardiac disease in the mouse on a clinical 3T scanner, a widely available platform.

Acknowledgements

This work was partially supported by the Swiss National Science Foundation (grant PPOOB3-116901) and the Center for Biomedical Imaging (CIBM), Lausanne and Geneva, Switzerland.

REFERENCES

1. Epstein FH. MR in mouse models of cardiac disease. NMR Biomed. 2007; 20(3): 238–255.
2. Jacquier A, Higgins CB, Saeed M. MR imaging in assessing cardiovascular interventions and myocardial injury. Contrast Media Mol. Imaging 2007; 2(1): 1–15.
3. Sakuma H. Magnetic resonance imaging for ischemic heart disease. J. Magn. Reson. Imaging. 2007; 26(1): 3–13.
4. Mendoncadias MH, Gaggelli E, Lauterbur PC. Paramagnetic Contrast Agents in Nuclear Magnetic-Resonance Medical Imaging. Sem. Nucl. Med. 1983; 13(4): 364–376.
5. Waghorn B, Edwards T, Yang Y, Chuang KH, Yanasak N, Hu TC. Monitoring dynamic alterations in calcium homeostasis by T (1)-weighted and T (1)-mapping cardiac manganese-enhanced MRI in a murine myocardial infarction model. NMR Biomed. 2008.
6. Lukyanenko V, Chikando A, Lederer WJ. Mitochondria in cardiomyocyte Ca2+ signaling. Int. J. Biochem. Cell. Biol. 2009; 41(10): 1957–1971.
7. Hu TC, Pautler RG, MacGowan GA, Koretsky AP. Manganese-enhanced MRI of mouse heart during changes in inotropy. Magn. Reson. Med. 2001; 46(5): 884–890.
8. Krombach GA, Saeed M, Higgins CB, Novikov V, Wendland MF. Contrast-enhanced MR delineation of stunned myocardium with administration of MnCl(2) in rats. Radiology. 2004; 230(1): 183–190.
9. Wendland MF. Applications of manganese-enhanced magnetic resonance imaging (MEMRI) to imaging of the heart. NMR Biomed. 2004; 17(8): 581–594.
10. Yang Y, Gruwel ML, Sun J, Gervai P, Yang X, Kupriyanov VV. Manganese-enhanced MRI of acute cardiac ischemia and chronic infarction in pig hearts: kinetic analysis of enhancement development. NMR Biomed. 2009; 22(2): 165–173.
11. Bremerich J, Saeed M, Arheden H, Higgins CB, Wendland MF. Normal and infarcted myocardium: differentiation with cellular uptake of manganese at MR imaging in a rat model. Radiology 2000; 216(2): 524–530.
12. Bruvold M, Nordhoy W, Anthonsen HW, Brurok H, Jynge P. Manganese-calcium interactions with contrast media for cardiac magnetic resonance imaging: a study of manganese chloride supplemented with calcium gluconate in isolated Guinea pig hearts. Invest. Radiol. 2005; 40(3): 117–125.
13. Hu TC, Bao W, Lenhard SC, Schaeffer TR, Yue TL, Willette RN, Jucker BM. Simultaneous assessment of left-ventricular infarction size, function and tissue viability in a murine model of myocardial infarction by cardiac manganese-enhanced magnetic resonance imaging (MEMRI). NMR Biomed. 2004; 17(8): 620–626.
14. Michael LH, Ballantyne CM, Zachariah JP, Gould KE, Pocius JS, Taffet GE, Hartley CJ, Pham TT, Daniel SL, Funk E, Entman ML. Myocardial infarction and remodeling in mice: effect of reperfusion. Am. J. Physiol. 1999; 277(2 Pt 2): H660–668.
15. Yang F, Liu YH, Yang XP, Xu J, Kapke A, Carretero OA. Myocardial infarction and cardiac remodelling in mice. Exp. Physiol. 2002; 87(5): 547–555.
16. Silva AC, Lee JH, Aoki I, Koretsky AP. Manganese-enhanced magnetic resonance imaging (MEMRI): methodological and practical considerations. NMR Biomed. 2004; 17(8): 532–543.
17. Kellman P, Arai AE, McVeigh ER, Aletras AH. Phase-sensitive inversion recovery for detecting myocardial infarction using gadolinium-delayed hyperenhancement. Magn. Reson. Med. 2002; 47(2): 372–383.
18. Daire JL, Hyacinthe JN, Tatar I, Montet-Abou K, Ivancevic MK, Masterson K, Jorge-Costa M, Morel DR, Vallee JP. In vivo myocardial infarct area at risk assessment in the rat using manganese enhanced magnetic resonance imaging (MEMRI) at 1.5T. Magn. Reson. Med. 2008; 59(6): 1422–1430.
19. Cerqueira MD, Weissman NJ, Dilsizian V, Jacobs AK, Kaul S, Laskey WK, Pennell DJ, Rumberger JA, Ryan T, Verani MS. Standardized myocardial segmentation and nomenclature for tomographic imaging of the heart: a statement for healthcare professionals from the Cardiac Imaging Committee of the Council on Clinical Cardiology of the American Heart Association. Circulation 2002; 105(4): 539–542.
20. Vivaldi MT, Kloner RA, Schoen FJ. Triphenyltetrazolium staining of irreversible ischemic injury following coronary artery occlusion in rats. Am. J. Pathol. 1985; 121(3): 522–530.
21. Simonetti OP, Kim RJ, Fieno DS, Hillenbrand HB, Wu E, Bundy JM, Finn JP, Judd RM. An improved MR imaging technique for the visualization of myocardial infarction. Radiology 2001; 218(1): 215–223.
22. Bohl S, Lygate CA, Barnes H, Medway D, Stork LA, Schulz-Menger J, Neubauer S, Schneider JE. Advanced methods for quantification of infarct size in mice using three-dimensional high-field late gadolinium enhancement MRI. Am. J. Physiol. Heart Circ. Physiol. 2009; 296(4): H1200–1208.
23. Mahoney JP, Small WJ. Studies on manganese. 3. The biological half-life of radiomanganese in man and factors which affect this half-life. J. Clin. Invest. 1968; 47(3): 643–653.
24. Kang YS, Gore JC. Studies of tissue NMR relaxation enhancement by manganese. Dose and time dependences. Invest. Radiol. 1984; 19(5): 399–407.
25. Ojha N, Roy S, Radtke J, Simonetti O, Gnyawali S, Zweier JL, Kuppusamy P, Sen CK. Characterization of the structural and functional changes in the myocardium following focal ischemia-reperfusion injury. Am. J. Physiol. Heart Circ. Physiol. 2008; 294(6): H2435–2443.
26. Yang Z, Berr SS, Gilson WD, Toufektsian MC, French BA. Simultaneous evaluation of infarct size and cardiac function in intact mice by contrast-enhanced cardiac magnetic resonance imaging reveals contractile dysfunction in noninfarcted regions early after myocardial infarction. Circulation 2004; 109(9): 1161–1167.
27. Oshinski JN, Yang Z, Jones JR, Mata JF, French BA. Imaging time after Gd-DTPA injection is critical in using delayed enhancement to determine infarct size accurately with magnetic resonance imaging. Circulation 2001; 104(23): 2838–2842.

28. Winter EM, Grauss RW, Atsma DE, Hogers B, Poelmann RE, van der Geest RJ, Tschope C, Schalij MJ, Gittenberger-de Groot AC, Steendijk P. Left ventricular function in the post-infarct failing mouse heart by magnetic resonance imaging and conductance catheter: a comparative analysis. Acta Physiol. (Oxf). 2008; 194(2): 111–122.
29. Bolli R, Marban E. Molecular and cellular mechanisms of myocardial stunning. Physiol. Rev. 1999; 79(2): 609–634.
30. Hampton TG, Amende I, Travers KE, Morgan JP. Intracellular calcium dynamics in mouse model of myocardial stunning. Am. J. Physiol. 1998; 274(5 Pt 2): H1821–1827.
31. Medina DC, Kirkland DM, Tavazoie MF, Springer CS Jr, Anderson SE. Na+/Ca2+-exchanger-mediated Mn2+-enhanced (1)H2O MRI in hypoxic, perfused rat myocardium. Contrast Media Mol. Imaging 2007; 2(5): 248–257.
32. Berry CJ, Thedens DR, Light-McGroary K, Miller JD, Kutschke W, Zimmerman KA, Weiss RM. Effects of deep sedation or general anesthesia on cardiac function in mice undergoing cardiovascular magnetic resonance. J. Cardiovasc. Magn. Reson. 2009; 11(1): 16.
33. Nayak KS, Hargreaves BA, Hu BS, Nishimura DG, Pauly JM, Meyer CH. Spiral balanced steady-state free precession cardiac imaging. Magn. Reson. Med. 2005; 53(6): 1468–1473.
34. Gilson WD, Yang Z, French BA, Epstein FH. Measurement of myocardial mechanics in mice before and after infarction using multislice displacement-encoded MRI with 3D motion encoding. Am. J. Physiol. Heart. Circ. Physiol. 2005; 288(3): H1491–1497.
35. Hyacinthe JN, Ivancevic MK, Daire JL, Vallee JP. Feasibility of complementary spatial modulation of magnetization tagging in the rat heart after manganese injection. NMR Biomed. 2008; 21(1): 15–21.
36. Epstein FH, Yang Z, Gilson WD, Berr SS, Kramer CM, French BA. MR tagging early after myocardial infarction in mice demonstrates contractile dysfunction in adjacent and remote regions. Magn. Reson. Med. 2002; 48(2): 399–403.
37. Zhou R, Pickup S, Glickson JD, Scott CH, Ferrari VA. Assessment of global and regional myocardial function in the mouse using cine and tagged MRI. Magn. Reson. Med. 2003; 49(4): 760–764.
38. Dornier C, Somsen GA, Ivancevic MK, Osman NF, Didier D, Righetti A, Vallee JP. Comparison between tagged MRI and standard cine MRI for evaluation of left ventricular ejection fraction. Eur. Radiol. 2004; 14(8): 1348–1352.
39. Natanzon A, Aletras AH, Hsu LY, Arai AE. Determining canine myocardial area at risk with manganese-enhanced MR imaging. Radiology 2005; 236(3): 859–866.